Gravity Compensation for PHANToM[TM] Omni® Haptic Interface

Majid H. Koul[†], Praneeth Kumar[#], Praveen K. Singh[*], M. Manivannan[#], Subir K. Saha[†]

[†] Department of Mechanical Engineering
Indian Institute of Technology Delhi
New Delhi - 110016, India
email: majid_me@student.iitd.ac.in,
saha@mech.iitd.ac.in

[#]Department of Applied Mechanics
Indian Institute of Technology Madras
Chennai - 600 036, India
e-mail: om.pran27@gmail.com,
mani@iitm.ac.in

[*] Scientist, Mechanical Engineering Research and Development Organization
(CSIR Govt. of India), Ludhiana-141006, India
email: praveen.mech.iitd@gmail.com

ABSTRACT

Although there have been many devices developed for Haptic applications, SensAble's PHANToM Omni and Desktop models have gained wide popularity among the researchers in Haptics community. Recent haptics application such as medical simulations, stroke rehabilitation, dental restorations, and others require attachments of additional equipments to the stylus of the Phantom in order to make it appear as realistic virtual environment. In any virtual reality application, the inertial and gravitational properties characterizing the haptic manipulator may represent a disturbance which can strongly affect the simulation realisms. In the scope of this research, we focus on the problem of compensating the apparent gravity acting on the end-effector, due to the gravitational contributions acting on the whole kinematic chain of the haptic device. In this paper, we present a kinematic and dynamic study of the PHANToM Omni Haptic interface and its implementation in gravity compensation technique. The kinematic analysis is carried out for the system and the dynamic analysis is carried out using the DeNOC methodology. The equations of motion and the expressions for the necessary torque at respective joints are established using the symbolic toolbox included in Matlab. The expression along with the necessary logic is implemented in the SensAble's Open Haptics Toolkit (HDAPI) software interface where the gravity compensation technique is carried out. The gravity compensation worked well, eliminating the effects of gravity even at the edges of the device workspace. The computational method used in this work is simple and can be used to calculate the compensation torques for various masses added to the end-effector.

Keywords: Force feedback devices, Virtual Reality, DeNOC.

1   INTRODUCTION

Although force feedback devices exist earlier than 1990s, the first successful force reflecting haptic interface device PHANToM, originally designed by Massie and Salisbury (1994) [1], and subsequently commercialized by SensAble Technologies, Inc.(Woburn, MA) [2], came into existence only in 1994. It is being widely used in a multitude of applications ranging from designing toys and footwear to research and robotic applications. Its wide use in the haptics community is predominantly due to its generic in nature, large workspace, low inertia, low friction and high position precision characteristics. However recent haptic applications such as medical simulations, stroke rehabilitation, dental restorations, and others require attachments of additional equipments or instruments to the end-effector or stylus of the PHANToM in order to make it appear realistic virtual environment. In any virtual reality application, the inertial and gravitational properties characterizing the haptic manipulator may represent a disturbance which can strongly affect the simulation realisms.

In the scope of this research, we focus on the problem of compensating the apparent gravity acting on the end-effector, due to the gravitational contributions acting on the whole kinematic chain of the haptic device. Several works can be found in the literature where different techniques have been employed in order to actively cancel the effects of gravity on haptic manipulators [3, 4, 5, 6, 7]. The commercially

available toolkit such as Open-Haptics does not provide tools for modifications of the Phantom dynamics, which requires a detailed knowledge of the system parameters of the haptics device not generally known to the end users.

In this paper, we present a detailed study of the mechanical properties of the PHANToM Omni haptic interface specifically for gravity compensation. Although, similar works have been reported on the PHANToM® premium models [8], we specifically focus here on the Omni model of the Phantom family. Here, we first derive and subsequently analyze the kinematics and the dynamic equations of motion for a generalized model of the device, assuming infinitely stiff joints and negligible friction. The solution is then applied to a particular case of PHANToM model. The established equations of motion are used in writing a program in SensAble's Open Haptics Toolkit [9] HDAPI (Haptic Device Application Programming Interface) in achieving gravity compensation for the device. The HDAPI provides low-level access to the haptic device, enabling haptics programmers to render forces directly. It offers control over configuring the runtime behaviour of the drivers, and provides convenient utility features and debugging aids.

In this paper, we use the notations used by Saha [10], in representing rigid body transformations, kinematics and dynamic equations. Dynamic analysis is carried out using the DeNOC methodology [14], which has proven to be computationally efficient. The analysis is implemented in the Open Haptics toolkit HDAPI [11] for achieving the gravity compensation. The units used are in Meter-Kilogram-Second (MKS), unless otherwise stated. Throughout the paper, parameters and measurements are based on the PHANToM Omni model.

2   KINEMATICS

In this section the kinematic analysis of the PHANToM Omni manipulator is performed. Although some of the results given here are already implemented in the SensAble's GHOST and Basic Input Output libraries, it is useful to have the explicit expressions for an open architecture, and to use in tasks and functions not supported in these libraries. In the following subsections, solutions of the forward and inverse kinematics are presented, followed by the calculation of the manipulator Jacobian and a basic analysis of the workspace.

2.1   Modeling

The architecture of the PHANToM Omni can be visualized as a 3-bar Revolute-Revolute-Revolute (*RRR)* spatial manipulator. The kinematic diagram is shown in Figure 1. With the base frame attached to the ground, the architecture can be easily described using the Denavit- Hartenberg (DH) parameters shown in Table 1.
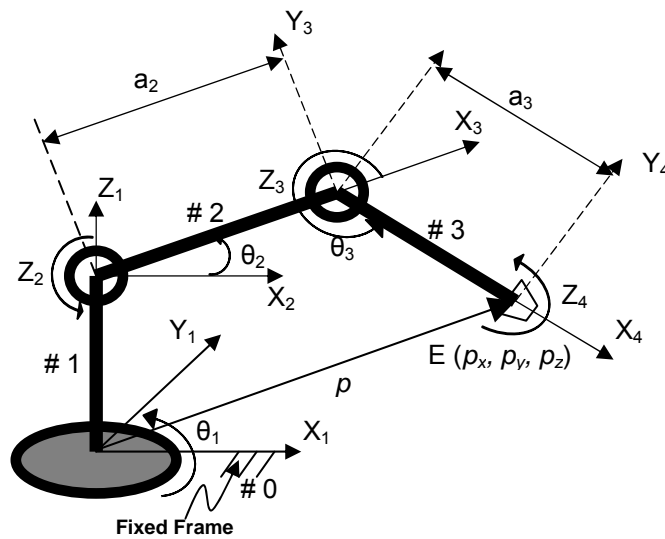

Figure 1. Kinematic diagram of PHANToM Omni.

Link #	b_i	θ_i (JV)	a_i	α_i
1	0	θ_1	0	$\pi/2$
2	0	θ_2	a_2	0
3	0	θ_3	a_3	0

Table 1. DH parameters

where, b_i : Joint offset, θ_i : Joint angle, a_i: Link length, α_i : Twist angle.

2.2 Forward Kinematics

The kinematic configuration of the manipulator is characterized by the following vectors:

$$\mathbf{e}_{ij} = \begin{bmatrix} 0 & 0 & 1 \end{bmatrix}^T ; \ \mathbf{a}_{ij} = \begin{bmatrix} a_i & 0 & 0 \end{bmatrix}^T , \text{ for } i = 1,2,3. \tag{1}$$

where, $\mathbf{e}_{ij}$ is the unit vector along i^{th} joint axes expressed in the jth frame for i = j; and $\mathbf{a}_{ij}$ is the position vector of ith link in j^{th} frame. Moreover, the transformation matrices representing the position and orientation of a coordinate frame with respect to its previous one are given by:

$$\mathbf{T}_1 = \begin{bmatrix} c_1 & 0 & s_1 & 0 \\ s_1 & 0 & -c_1 & 0 \\ 0 & 1 & 0 & 0 \\ 0 & 0 & 0 & 1 \end{bmatrix} ; \ \mathbf{T}_i = \begin{bmatrix} c_i & -s_i & 0 & a_i c_i \\ s_i & c_i & 0 & a_i s_i \\ 0 & 0 & 1 & 0 \\ 0 & 0 & 0 & 1 \end{bmatrix} , \text{ for } i = 2, 3. \tag{2}$$

where, $\mathbf{T}_i$ is the transformation matrix of the frame attached to body i, i.e. frame $i+1$, represented in frame i attached to the body (i-1). The terms s_i and c_i, for i = 1, 2, 3, represent $\sin\theta_i$ and $\cos\theta_i$, respectively.

The homogeneous transformation matrix of the end-effector frame with respect to the fixed frame is then given by:

$$\mathbf{T} = \mathbf{T}_1 \mathbf{T}_2 \mathbf{T}_3 \tag{3}$$

i.e.,

$$\mathbf{T} = \begin{bmatrix} c_1 c_{23} & -c_1 s_{23} & -s_1 & c_1(a_2 c_2 + a_3 c_{23}) \\ s_1 c_{23} & -s_1 s_{23} & c_1 & s_1(a_2 c_2 + a_3 c_{23}) \\ -s_{23} & -c_{23} & 0 & -(a_2 s_2 + a_3 s_{23}) \\ 0 & 0 & 0 & 1 \end{bmatrix} \tag{4}$$

From equation (4), the forward kinematics map is given by:

$$p_x = c_1(a_2 c_2 + a_3 c_{23}) ; \ p_y = s_1(a_2 c_2 + a_3 c_{23}) ; \ p_z = -(a_2 s_2 + a_3 s_{23}) ; \tag{5}$$

where, p_x, p_y and p_z are the components of the positions of the end-effector, i.e., point E in Figure 1.

The isometric workspace in the XZ plane and the reachable boundary in YZ plane for the measured parameters given in Appendix are shown in Figures 2(a) and 2(b), respectively.
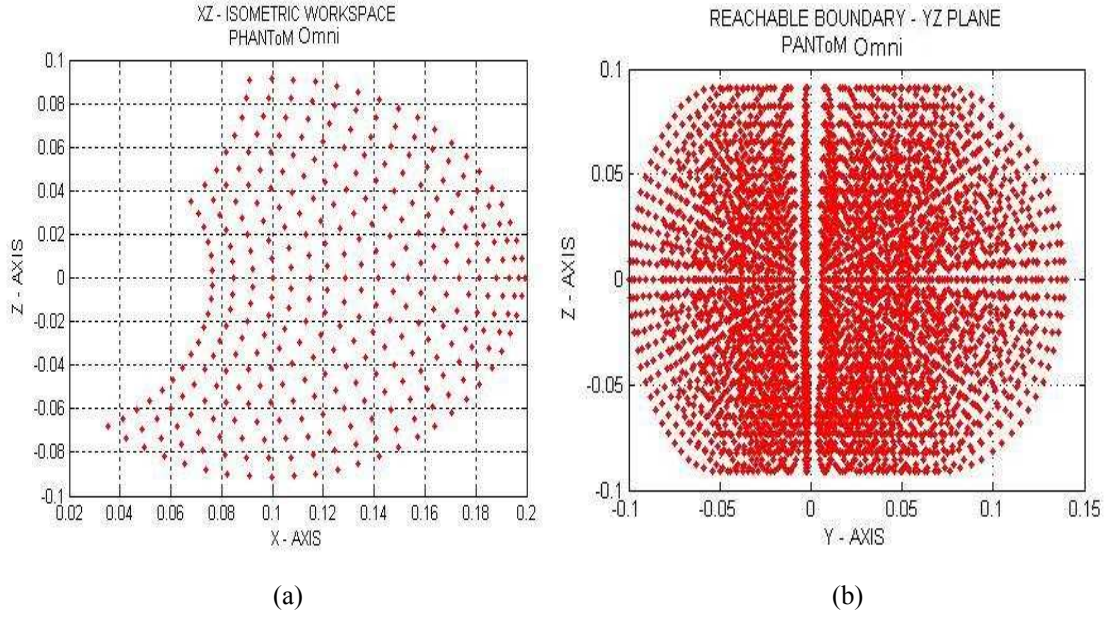
Figure 2. Workspace of Phantom Omni

2.3   Inverse Kinematics

As this is a 3-degrees of freedom (DOF) manipulator, its inverse kinematics problem is to find θ_1, θ_2 and θ_3 which would move the manipulator to a desired end-effector position, i.e.,

$$\mathbf{p}(\boldsymbol{\theta}) = \begin{bmatrix} p_x & p_y & p_z \end{bmatrix}^T \tag{6}$$

where $\boldsymbol{\theta}$ represents the vector of joint positions $\theta \equiv \begin{bmatrix} \theta_1 & \theta_2 & \theta_3 \end{bmatrix}^T$.
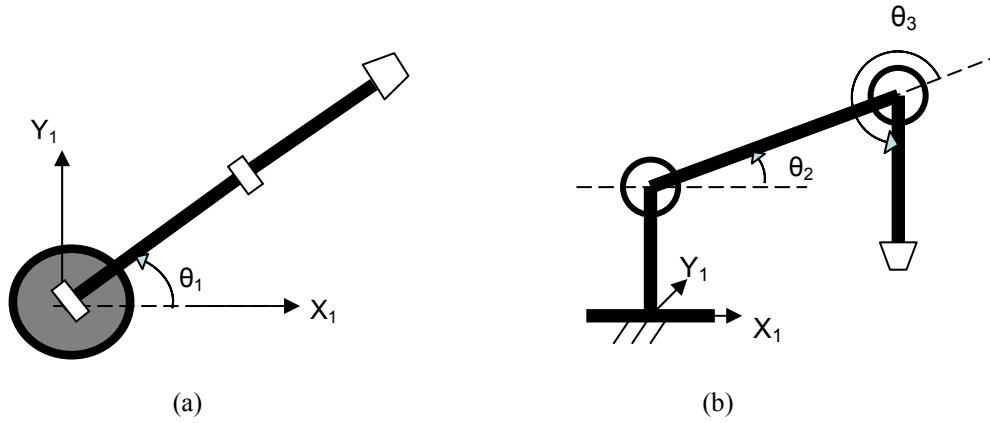

Figure 3. Manipulandum top and side views

Note that θ_1 can be determined by inspection from the top view of Figure 3(a), whereas the angles θ_2 and θ_3 are determined from the geometry of Figure 3(b) and are given by:

$$\theta_1 = \text{atan2}\,(p_y, p_x)\;;\; \Delta \equiv p_x^2 + p_y^2 + p_z^2 \tag{7}$$

$$\theta_2 = -\sin^{-1}\left[\frac{(a_2 + a_3 c_3)p_z + a_3 s_3 \sqrt{p_x^2 + p_y^2}}{\Delta} \right] \tag{8}$$

$$\theta_3 = \cos^{-1}\left[\frac{p_x^2 + p_y^2 + p_z^2 - a_2^2 - a_3^2}{2a_2 a_3}\right] \tag{9}$$

Since the model is conceptually a 3-RRR spatial manipulator, it has four admissible inverse kinematic solutions. As for the PHANToM Omni interface, the constraints imposed lead to a particular set of inverse kinematic solution only.

2.4 Manipulator Jacobian

In order to obtain the Manipulator Jacobian, the end-effector twist [13] is defined as the 6-dimensional vector array of angular velocity and linear velocity of the end-effector, namely, E of Figure 1. The Jacobian relates the twist with its joint rate vector $\dot{\boldsymbol{\theta}}$ as

$$\mathbf{t} = \mathbf{J}\,\dot{\boldsymbol{\theta}} \tag{10}$$

where $\mathbf{J}$ is the Jacobian matrix, or simply Jacobian. It is the 6 x 3 matrix given by

$$\mathbf{J} \equiv \begin{bmatrix} 0 & -s_1 & -s_1 \\ 0 & c_1 & c_1 \\ 1 & 0 & 0 \\ -s_1(a_2c_2 + a_3c_{23}) & -c_1(a_2s_2 + a_3s_{23}) & -a_3c_1s_{23} \\ c_1(a_2c_2 + a_3c_{23}) & -s_1(a_2s_2 + a_3s_{23}) & -a_3s_1s_{23} \\ 0 & -(a_2c_2 + a_3c_{23}) & -a_3c_{23} \end{bmatrix} \tag{11}$$

Since the Phantom Omni has only 3-DOF force feedback, the last three rows of $\mathbf{J}$ are relevant. Hence, the Jacobian resulting from the last three rows, which is denoted by $\mathbf{J}_l$ can be used for singularity and other studies. Note that apart from boundary singularities, the system has no singularity inside its workspace.
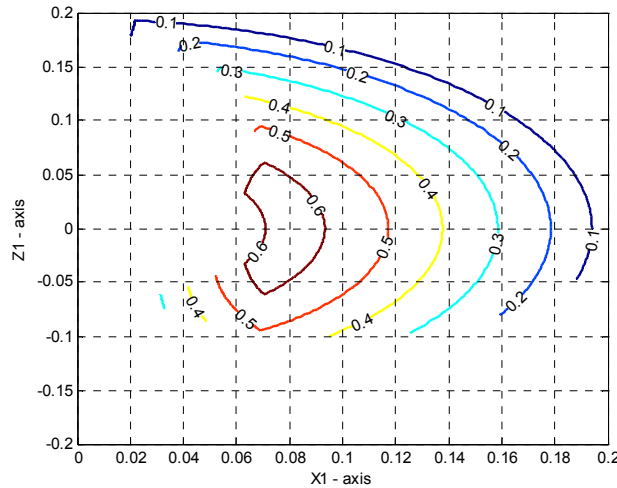
2.5 Manipulability

Figure 4. Manipulability graph for Phantom Omni

The manipulability measure used here is defined from [13] as

$$\mu = \sigma_{\min}(\mathbf{J}_l) / \sigma_{\max}(\mathbf{J}_l) \tag{12}$$

where σ_{min} and σ_{max} are the minimum and maximum singular values, and $\mathbf{J}_l$ is the 3x3 Jacobian matrix that corresponds to the positioning of end-effector, E of Figure 1, only. This measure is based on the 2-norm condition number, as shown in Figure 4. The plots reveal that the Phantom Omni interface has a singularity-free workspace with quite uniform manipulability over a significant portion of the workspace, which is a favorable kinematic property.

3   DYNAMICS

It is necessary to know the dynamic equations of motion of the Phantom Omni to implement the high performance controllers such as gravity compensation or the computed torque control algorithm. The dynamic equations of motion governing the motion of the serial 3-RRR spatial manipulator are derived here using the Newton-Euler equations of motion for the rigid bodies and the corresponding Decoupled Natural Orthogonal Complement (DeNOC) matrices. The DeNOC matrices relate the angular and linear velocities of the rigid bodies in the system to the associated joint rates.

For the angular velocity of a rigid link say, $i, \boldsymbol{\omega}_i$, and its linear velocity of the mass centre $\dot{\mathbf{c}}_i$, the twist, $\mathbf{t}_i$, is defined as the 6-dimensional vector as

$$\mathbf{t}_i \equiv \begin{bmatrix} \boldsymbol{\omega}_i \\ \dot{\mathbf{c}}_i \end{bmatrix} \tag{13}$$

Accordingly, if the moment and the force acting on the rigid link are denoted with $\mathbf{n}_i$ and $\mathbf{f}_i$, respectively, the 6-dimensional vector of wrench, $\mathbf{w}_i$, is defined by

$$\mathbf{w}_i \equiv \begin{bmatrix} \mathbf{n}_i \\ \mathbf{f}_i \end{bmatrix} \tag{14}$$

Next, the Newton Euler equations of motion for the ith rigid link is written in compact form as

$$\mathbf{M}_i \dot{\mathbf{t}}_i + \mathbf{W}_i \mathbf{M}_i \mathbf{t}_i = \mathbf{w}_i \tag{15}$$

where the left hand side of the above equation is associated with the inertia wrenches which is equated to external wrenches. The 6×6 matrices of the mass, $\mathbf{M}_i$, and of the angular velocity, $\mathbf{W}_i$, are defined as

$$\mathbf{M}_i \equiv \begin{bmatrix} \mathbf{I}_i & \mathbf{O} \\ \mathbf{O} & m_i \mathbf{1} \end{bmatrix}, \ \mathbf{W}_i \equiv \begin{bmatrix} \tilde{\boldsymbol{\omega}}_i & \mathbf{O} \\ \mathbf{O} & \mathbf{O} \end{bmatrix} \tag{16}$$

where $\mathbf{M}_i$ is the mass matrix that embodies the mass and inertia properties of the ith body about the center of mass (C_i). The unconstrained NE equation of motion for the complete system are then written as

$$\mathbf{M}\dot{\mathbf{t}} + \mathbf{W}\mathbf{M}\mathbf{t} = \mathbf{w} \tag{17}$$

where the $6n \times 6n$ matrices – n being the number of links in the serial system and also the degree of freedom (DOF) as there are n-joints to connect the n links serially, $\mathbf{M}$ and $\mathbf{W}$ are the generalized mass and angular velocity matrix respectively, namely

$$\mathbf{M} \equiv diag\begin{bmatrix} \mathbf{M}_1, & \cdots, & \mathbf{M}_n \end{bmatrix}, \ \mathbf{W} \equiv diag\begin{bmatrix} \mathbf{W}_1, & \cdots, & \mathbf{W}_n \end{bmatrix} \tag{18}$$

Also, the $6n$-dimensional vectors of the generalized twist and wrench are given as

$$\mathbf{t} \equiv \begin{bmatrix} \mathbf{t}_1, & \cdots, & \mathbf{t}_n \end{bmatrix}^T, \ \mathbf{w} \equiv \begin{bmatrix} \mathbf{w}_1, & ..., & \mathbf{w}_n \end{bmatrix}^T \tag{19}$$

The generalized twist of the system is then expressed in compact form as

$$\mathbf{t} \equiv \mathbf{N}\,\dot{\boldsymbol{\theta}}, \text{ where } \mathbf{N} \equiv \mathbf{N}_l \mathbf{N}_d \tag{20}$$

where $\mathbf{N}$ is the Natural Orthogonal Complement (NOC) matrix [15] of $6n \times n$ dimension, and $\mathbf{N}_l$, $\mathbf{N}_d$ are the DeNOC matrices [14]. The $6n \times 6n$ and $6n \times n$ block matrices $\mathbf{N}_l$ and $\mathbf{N}_d$ are expressed as

$$\mathbf{N}_l \equiv \begin{bmatrix} \mathbf{1} & \mathbf{O} & \cdots & \mathbf{O} \\ \mathbf{B}_{21} & \mathbf{1} & \cdots & \mathbf{O} \\ \vdots & \vdots & \ddots & \vdots \\ \mathbf{B}_{n1} & \mathbf{B}_{n2} & \cdots & \mathbf{1} \end{bmatrix}, \mathbf{N}_d \equiv \begin{bmatrix} \mathbf{p}_1 & \mathbf{O} & \cdots & \mathbf{O} \\ \mathbf{O} & \mathbf{p}_2 & \vdots & \mathbf{O} \\ \vdots & \vdots & \ddots & \vdots \\ \mathbf{O} & \mathbf{O} & \cdots & \mathbf{p}_n \end{bmatrix} \tag{21}$$

where, $\dot{\boldsymbol{\theta}} \equiv \begin{bmatrix} \dot{\theta}_1 & \dot{\theta}_2 & \cdots & \dot{\theta}_n \end{bmatrix}^T$, $\mathbf{p}_i$ is the joint-rate propagation vector and $\mathbf{B}_{ij}$ is the is the twist propagation matrix. They are given by

$$\mathbf{p}_i \equiv \begin{bmatrix} \mathbf{e}_i \\ \mathbf{e}_i \times \mathbf{d}_i \end{bmatrix}, \mathbf{B}_{ij} \equiv \begin{bmatrix} \mathbf{1} & \mathbf{O} \\ \tilde{\mathbf{c}}_{ij} & \mathbf{1} \end{bmatrix} \tag{22}$$

where $\mathbf{e}_i$ is the 3-dimensional unit vector parallel to the axis of rotation for a revolute joint and $\mathbf{d}_i$ is the 3-dimensional position vector of the mass center $\mathbf{c}_i$ from the ith joint location and $\tilde{\mathbf{c}}_{ij}$ is the skew symmetric matrix associated with the cross product of the vector joining the mass centers of links i and j. Now, pre-multiplying the transpose of the DeNOC matrices to the unconstrained NE equations of motion for the system in equation (17), the following set of constrained independent dynamic equations of motion are obtained:

$$\mathbf{I}\,\ddot{\boldsymbol{\theta}} + \mathbf{h} = \boldsymbol{\tau}, \text{ where } \mathbf{h} \equiv \mathbf{C}\dot{\boldsymbol{\theta}} \tag{23}$$

where, $\mathbf{I} \equiv \mathbf{N}^T \mathbf{M} \mathbf{N}$: the n x n Generalized Inertia Matrix, which is symmetric and positive definite;

$\mathbf{C} \equiv \mathbf{N}^T (\mathbf{M}\dot{\mathbf{N}} + \mathbf{W}\mathbf{M}\mathbf{N})$: the n x n Matrix of Convective Inertia (MCI) terms;

$\mathbf{h} \equiv \mathbf{C}\dot{\boldsymbol{\theta}}$: the n-dimensional Vector of Convective Inertia (VCI) terms;

$\boldsymbol{\tau} \equiv \boldsymbol{\tau}^e + \boldsymbol{\tau}^g$, where $\boldsymbol{\tau}^e = \mathbf{N}^T \mathbf{w}^E$ and $\boldsymbol{\tau}^g = \mathbf{N}^T \mathbf{w}^G$ are the 6-dimensional vector of generalized forces due to the driving torques/forces, and those resulting from gravity respectively.

The advantage of using DeNOC methodology enables estimation of the elements of the Generalized Inertia Matrix (GIM), MCI and the 6-dimensional vectors of generalized forces recursively [10]. Using equation (23), the expression for torque can be obtained for inverse dynamics, i.e., for a given trajectory at the joints, the necessary torque needed to counteract the gravitational effects can be obtained. The detailed expressions for the dynamics are given in the Appendix.

4   EXPERIMENTAL EVALUATIONS

Several validation experiments have been performed by applying the proposed algorithm to Omni model of Phantom family. This was based on the estimation of the gravity at the desired position of the workspace and providing the equal but opposite torques at the joint motors. This may be useful for those not interested in force accuracy, perhaps designers or such like, but it is appropriate for our uses. The following are the considerations made for implementing the gravity compensation:

4.1   Calculation of masses and lengths

A similar Phantom Omni was dismantled [12] and the masses of the required parts were measured using an electronic weighing scale. Calculation of the centre of masses and the moments of inertia was done using approximations. Since these values can vary slightly from device to device we have analyzed and coded using variables and have substituted for them appropriately to obtain the final results. Hence the analyses can be used for other 3-DOF devices by assigning the appropriate values for the parameters.

4.2 Torque calculations

The expressions for the torques that act on different motors were obtained using the DeNOC-based methodology. Study of the internal mechanism of the Phantom Omni [12] showed that the torque was transmitted using a metallic wire and the torque given by the motors was amplified by winding the thread over a segment of disc. Therefore, the anti-torque values given to the motors were multiplied by the amplification factor. The ratio of the radius of the shaft to the radius of the disc is 0.125 and hence the torque amplification factor is 0.125. This is true for both the arms of the Phantom Omni. During the entire analysis the frictional effects have not been considered. They could be accounted for by multiplying the torques by appropriate factors. This is completely device dependent. Hence these values can vary from device to device. We are using a factor of 1 for motor 2 and a factor of 8 for motor 3.

4.3 Conversion of torque to DAC values

The assignment of torques to the motors was achieved using Digital to Analog (DAC) values. We have assumed a linear relationship between the DAC values and the torques. The constant for linearization was obtained by dividing the maximum allowable value of DAC with the maximum permissible torque for Phantom Omni. The end-effector was moved to different locations within the workspace with different velocity using hands and left at the location to check if its location was changing. The location did not change even at the edges of the workspace. Hence the gravity compensation scheme worked successfully.

5 CONCLUSIONS

In this work we derived dynamic equations of motion of the Omni model of Phantom. Along with the approximation of inertial parameters of each of the links, we were able to implement a gravity compensation control scheme. The gravity compensation worked very well, eliminating the effects of the gravity even at the edges of the phantom workspace. We have also successfully implemented other control strategies, such as the computed torque algorithm, that rely on the use of accurate dynamic equations.

The computational method used in this work is simple and can be used to calculate the compensation torques for various masses added to the end-effector. It does not involve any iterative control strategy such as in [3]. Our method does not need to approximate the whole workspace to grids and sample for kinematics as described in their work. The experimental results are in good agreement with the theoretical derivation.

Although this paper focused on the kinematics and dynamics of the Phantom Omni, much of the results and analysis apply to the Phantom Desktop, due to the similarity in the kinematics of both models, with obvious variations in the parameter values.

ACKNOWLEDGEMENT

APPENDIX

Non-zero elements of matrix N for 3-DOF Phantom Omni are (18 rows; 3 columns):

$$N_{3,1} = N_{9,1} = N_{15,1} = 1, \ N_{8,2} = N_{14,2} = N_{14,3} = c_1, \ N_{7,2} = N_{13,2} = N_{13,3} = -s_1,$$

$$N_{12,2} = -\left(a_2\, c_2\, / 2\right), \ N_{10,1} = N_{10,2} = -\left(a_2\, s_1 c_2\, / 2\right), \ N_{11,1} = \left(a_2\, c_1 c_2\, / 2\right),$$

$$N_{11,2} = -\left(a_2\, s_1 s_2\, / 2\right), \ N_{16,1} = -a_2\, s_1 c_2 - \left(a_3\, s_1 c_{23}\, / 2\right), \ N_{17,1} = a_2\, c_1 c_2 + \left(a_3\, c_1 c_{23}\, / 2\right),$$

$$N_{16,2} = -\left(a_2\, s_2 \left(1 + c_1\right) / 2\right) - \left(a_3\, c_1 s_{23}\, / 2\right), \ N_{17,2} = -a_2\, s_1 s_2 - \left(a_3\, s_1 s_{23}\, / 2\right),$$

$$N_{16,3} = -\left(a_3\, c_1 s_{23}\, / 2\right), \ N_{17,3} = -\left(a_3\, s_1 s_{23}\, / 2\right), \ N_{18,2} = -a_2\, c_2 - \left(a_3\, c_{23}\, / 2\right),$$

$$N_{18,3} = \left(a_3\, c_{23} \,/\, 2\right).$$

Non-zero elements of matrix M

$$M_{7,7} = c^2_1 \left(I_{2xx} c^2_2 + I_{2yy} s^2_2\right) + I_{2zz} s^2_1, \quad M_{7,8} = M_{8,7} = s_1 c_1 \left(I_{2xx} c^2_2 + I_{2yy} s^2_2\right) - I_{2zz} s_1 c_1,$$

$$M_{7,9} = M_{9,7} = - c_1 c_2 s_2 \left(I_{2xx} - I_{2yy}\right), \quad M_{8,8} = s^2_1 \left(I_{2xx} c^2_2 + I_{2yy} s^2_2\right) + I_{2zz} c^2_1,$$

$$M_{8,9} = M_{9,8} = - s_1 s_2 c_2 \left(I_{2xx} - I_{2yy}\right), \quad M_{9,9} = \left(I_{2xx} s^2_2 + I_{2yy} c^2_2\right),$$

$$M_{10,10} = M_{11,11} = M_{12,12} = m_2, \quad M_{13,13} = c^2_1 \left(I_{3xx} c^2_{23} - I_{3yy} s^2_{23}\right) + I_{3zz} s^2_1,$$

$$M_{13,14} = M_{14,13} = s_1 c_1 \left(I_{3xx} c^2_{23} + I_{3yy} s^2_{23}\right) - I_{3zz} s_1 c_1,$$

$$M_{13,15} = M_{15,13} = c_1 s_{12} c_{12} \left(- I_{3xx} + I_{3yy}\right), \quad M_{14,14} = s^2_1 \left(I_{3xx} c^2_{23} + I_{3yy} s^2_{23}\right) + I_{3zz} c^2_1,$$

$$M_{14,15} = M_{15,14} = - s_1 s_{23} c_{23} \left(I_{3xx} - I_{3yy}\right), \quad M_{15,15} = I_{3xx} s^2_{23} + I_{3yy} c^2_{23},$$

$$M_{16,16} = M_{17,17} = M_{18,18} = m_3.$$

Non-zero elements of matrix W

$$W_{1,2} = - W_{2,1} = - W_{7,8} = W_{8,7} = - W_{13,14} = W_{14,13} = \dot{\theta}_1; \quad W_{7,9} = - W_{9,7} = c_1 \dot{\theta}_2.$$

$$W_{8,9} = - W_{9,8} = s_1 \dot{\theta}_2; \quad W_{13,15} = - W_{15,13} = \left(\dot{\theta}_2 + \dot{\theta}_3\right) c_1; \quad W_{14,15} = - W_{15,14} = \left(\dot{\theta}_2 + \dot{\theta}_3\right) s_1.$$

Elements of vector τ^g

$$\tau^g_1 = 0; \quad \tau^g_2 = 0.5\mathbf{g} \left(2a_2\, m_2 c_2 + 3a_2\, m_3 c_2 + a_3\, m_3 c_{23}\right); \quad \tau^g_3 = 0.5\mathbf{g} \left(a_3\, m_3 c_{23}\right).$$

Inertial Parameters:

The spatial frame used in dynamic analysis is centered at the base of the system identified in Figure 1. The notation followed is similar to the one used by Saha [10]. To calculate the inertial parameters for the system, the links have been assumed to be of cylindrical in nature with the diameter of the cylinder comparatively smaller than its length.

Link lengths:

$a_2 = 0.135$m, $a_3 = 0.135$m.

Mass of links:

$m_2 = 0.035$ kg; $m_3 = 0.1$ kg (including the stylus attached to the end effector).

Torque magnification factor (through inextensible string pulled over a disc) = 8.

Moment of Inertia:

$$I_2 = \begin{bmatrix} I_{2xx} & 0 & 0 \\ 0 & I_{2yy} & 0 \\ 0 & 0 & I_{2zz} \end{bmatrix}; I_3 = \begin{bmatrix} I_{3xx} & 0 & 0 \\ 0 & I_{3yy} & 0 \\ 0 & 0 & I_{3zz} \end{bmatrix}.$$

$I_{2xx} = 0$, $I_{2yy} = 2.126 \times 10^{-4}$ kgm^2, $I_{2zz} = 2.126 \times 10^{-4}$ kgm^2 ; $I_{3xx} = 0$, $I_{3yy} = 6.075 \times 10^{-4}$ kgm^2, $I_{3zz} = 6.075 \times 10^{-4}$ kgm^2.

Range of joint variables:

$\theta_1 = -40^\circ - 60^\circ$; $\theta_2 = 0^\circ - 100^\circ$; θ_3 varies as θ_2 moves from $0^\circ - 100^\circ$ (mechanical constraint provided)

$\theta_3 = -140^\circ$ to -10° at $\theta_2 = 0^\circ$, and -140° to -95° at $\theta_2 = 100^\circ$, a linear relation was used to approximate the variation.

REFERENCES

[1] MASSIE, T. H. AND SALISBURY, J. K. The PHANToM haptic interface: A device for probing virtual objects. In *Proceedings of the ASME Winter Annual Meeting, Symposium on Haptic Interfaces for Virtual Environment and Teleoperator Systems.* Chicago, IL, 1994.

[2] http://www.sensable.com/, Website for SensAble Technologies.

[3] ALESSANDRO FORMAGLIO, MARCO FEI, SARA MULATTO, MAURIZIO DE PASCALE AND DOMENICO PRATTICHIZZO. *Autocalibrated Gravity Compensation for 3DoF Impedance Haptic Devices* - Lecture Notes in Computer Science, Springer Berlin / Heidelberg.

[4] BABAK TAATI, AMIR M. TAHMASEBI, KEYVAN HASHTRUDI-ZAAD. Experimental Identification and Analysis of the Dynamics of a PHANToM Premium 1.5A Haptic Device - *Presence* - August 2008, Vol. 17, No. 4, Pages 327-343.

[5] CHECCACCI, D. SOTGIU, E. FRISOLI, A. AVIZZANO, C.A. BERGAMASCO, M. Gravity Compensation algorithms for parallel haptic interface, pp. 140-145 – *Proceedings of the 2002 IEEE Int. Workshop on Robot and Human Interactive Communication,* 2002.

[6] OTT, R., GUTIERREZ, M., THALMANN, D., VEXO, F. Improving user comfort in Haptic virtual environments through gravity compensation - *Proceedings of the First Joint Eurohaptics Conference and Symposium on Haptic Interfaces for Virtual Environment and Teleoperator Systems* , 2005.

[7] FEDDEMA, J. T., NOVAK, J. L. Whole arm obstacle avoidance for teleoperated robots, pp. 3303-3309 - *Proceedings of IEEE International Conference on Robotics and Automation*, 1994.

[8] CAVUSOGLU M.. C., FEYGIN D, TENDICK F. A critical study of the mechanical and electrical properties of the PHANToM™ haptic interface and improvements for high performance control - *Presence*, 2002.

[9] http://www.sensable.com/products-openhaptics-toolkit.htm.

[10] SAHA, S. K. *Introduction to Robotics* (First Reprint) Tata McGraw-Hill, New Delhi India, 2009.

[11] *Ghost SDK Programmer's Guide Version 3.0* SenseAble Technologies Inc. 1997

[12] SensAble Technologies. *PHANToM(TM) haptic interface hardware installation and technical manual.* Cambridge, MA. (Revision 5.1), 1997.

[13] CRAIG J. J. *Introduction to robotics* (Second edition). Addison-Wesley. Reading, MA, 1989.

[14] SAHA, S. K. Dynamics of Serial Multibody systems using the Decoupled Natural Orthogonal Complement matrices – *ASME J. Appl. Mech*., 66, pp. 986-996, 1999.